Metals and Materials International (2023) 29:1195–1201
https://doi.org/10.1007/s12540-022-01282-w

Achieving Ultra-High-Strength and Good Ductility of the ZK60 Alloy Sheet by High Strain-Rate Rolling

Songhui Wang[1] · Wencong Zhang[1] · Jianlei Yang[1] · Xeuyan Jiao[3] · Jinqi Pan[1] · Guannan Chu[1] · Xiangyu Dai[1,2]

Received: 4 July 2022 / Accepted: 18 July 2022 / Published online: 1 September 2022

Abstract
A superior combination of the ultra-high tensile strength (~419.9 MPa), the yield strength (~376.9 MPa) and the elongation (~14.8%) ZK60 sheet was successfully achieved by high-strain rate rolling. The ultrahigh strength was attributed to the uniform ultrafine-grained structure. The excellent ductility was ascribed to the ultrafine grains, low dislocation density and weakened basal texture in the final structure.

Keywords Mg alloy · Ultrahigh-strength · Fine-grain · Texture · High strain-rate rolling

1 Introduction

Wrought magnesium alloys were the most popular lightweight materials in aerospace and electronics fields due to their low density, high specific strength and high specific stiffness [1, 2]. However, its low strength and poor plasticity at room temperature seriously limit its further wide application due to the hexagonal close-packed (HCP) structure [3, 4]. Therefore, improving the mechanical properties of the Mg alloys was important in expanding its application. It was well known that severe plastic deformation can significantly refine grains to obtain good mechanical properties (eg. equal channel angular pressing (ECAP) [5], high-pressure torsion, (HPT) [6] and high strain-rate rolling (HSRR) [7], etc.). Among them, the processes of the ECAP and HPT were complex and have many disadvantages, such as a long production cycle and high energy consumption. These factors limit their wide application.

In comparison, the high efficiency, short process and low energy consumption of HSRR were suitable for technological production and it has been applied to the preparation of Mg alloys and Al alloys [7–10]. For example, Xu and Jiang et al. [8, 9] reported the preparation of ultra-fine lamellar structure AM60 and ZM61 alloy sheets by HSRR, and the improvement of mechanical properties was mainly determined by grain refinement and precipitate hardening. Similarly, Yan et al. [10, 11] showed that commercial Mg alloys with balanced strength and plasticity could be successfully prepared by HSRR. In addition, Li et al. [12] reported that 5A12 Al alloy obtained excellent mechanical properties by HSRR. However, the initial materials used in these reports were all in the as-cast or homogenized state, which was not conducive to subsequent processing, because it was easy to crack in the HSRR process.

In this study, the ZK60 sheet was prepared by a single pass HSRR. The evolution of microstructure and texture as well as the change of properties, especially the influencing factors on strength were studied.

2 Experimental Procedures

The initial alloy was the hot-extruded ZK60 (Mg-6.63Zn-0.56Zr, wt.%) sheet (the specific extrusion process of the ZK60 sheet was as follows: the rod with a diameter of 100 mm was preheated at 350 ℃ for 30 min and then extruded to plate at 350 ℃ with 20,000 × 100 × 3 mm.

✉ Jianlei Yang
jlyang@hit.edu.cn

✉ Xiangyu Dai
hit_dxy0114@163.com

[1] School of Materials Science and Engineering, Harbin Institute of Technology, Harbin 150001, People's Republic of China

[2] State Key Laboratory of Advanced Welding and Joining, Harbin Institute of Technology, Harbin 150001, People's Republic of China

[3] School of Naval Architecture and Port Engineering, Shandong Jiaotong University, 1508 Hexing Road, Weihai 264310, People's Republic of China

Particularly, the extrusion ratio and die-exit speeds were 26.1 and 1.5 mm/s, respectively). The sheet with the size of 200 × 100 × 3 mm was preheated at 300 ℃ for 15 min and then processed by a single pass HSRR, with a strain rate of 11.3 s^{-1}, and a reduction of 50%. More specifically, the rolling direction (RD) was parallel to the extrusion direction (ED), and water quenching was conducted to retain the as-deformed microstructure.

Tension tests were performed on the Instron 5967 with a strain rate of 1×10^{-3} s^{-1} at room temperature (the initial alloy was loaded along the ED, and the HSRRed sheet was loaded along the RD). In order to ensure the repeatability of experimental results, three experiments were conducted for each state. The tensile specimens were machined along with ED/RD by wire cutting, and the dimension of the specimens was 15 mm × 4.0 mm × 1.5 mm. Microstructures and textures were analyzed by electron backscatter diffraction (EBSD). The EBSD samples were prepared by mechanical polishing and followed by electropolishing (5:3 C_2H_5OH and H_3PO_4 electrolyte, electropolishing for 2 min at 0.5 A and 5 min at 0.25 A). The orientation imaging microscopy software of TSLOIM Analysis 7.2 was utilized for data analysis.

3 Results and Discussion

Figure 1a shows the stress–strain curves of the ZK60 sheets at room temperature. It can be seen that the initial sheet has a relatively good combination of strength and ductility. And the ultimate tensile strength (UTS), the yield strength (YS), and the elongation (EL) were 323.2 ± 2 MPa, 229.5 ± 3 MPa and 28.7 ± 0.9%, respectively. Noted that the strength of the alloy would be substantially improved after HSRR. The HSRRed sheet exhibited the ultra-high UTS (419.9 ± 3 MPa), the YS (376.9 ± 4 MPa) and excellent the EL (14.8 ± 1.2%). As was known to all, the Hall–Petch relationship was widely used to quantify the strengthening contribution from grain size. It can be learned from the Hall–Petch relationship that the yield strength increases as the grain size decreases: $\sigma_{0.2} = \sigma_0 + kd^{-1/2}$ (σ_0 was the frictional stress for dislocation movement). In this work, in order to conveniently roughly quantify the Hall–Petch strengthening effect of the initial and HSRRed alloys, we assume that the yield strength of the alloys was only affected by grain size, without considering the effects of other factors

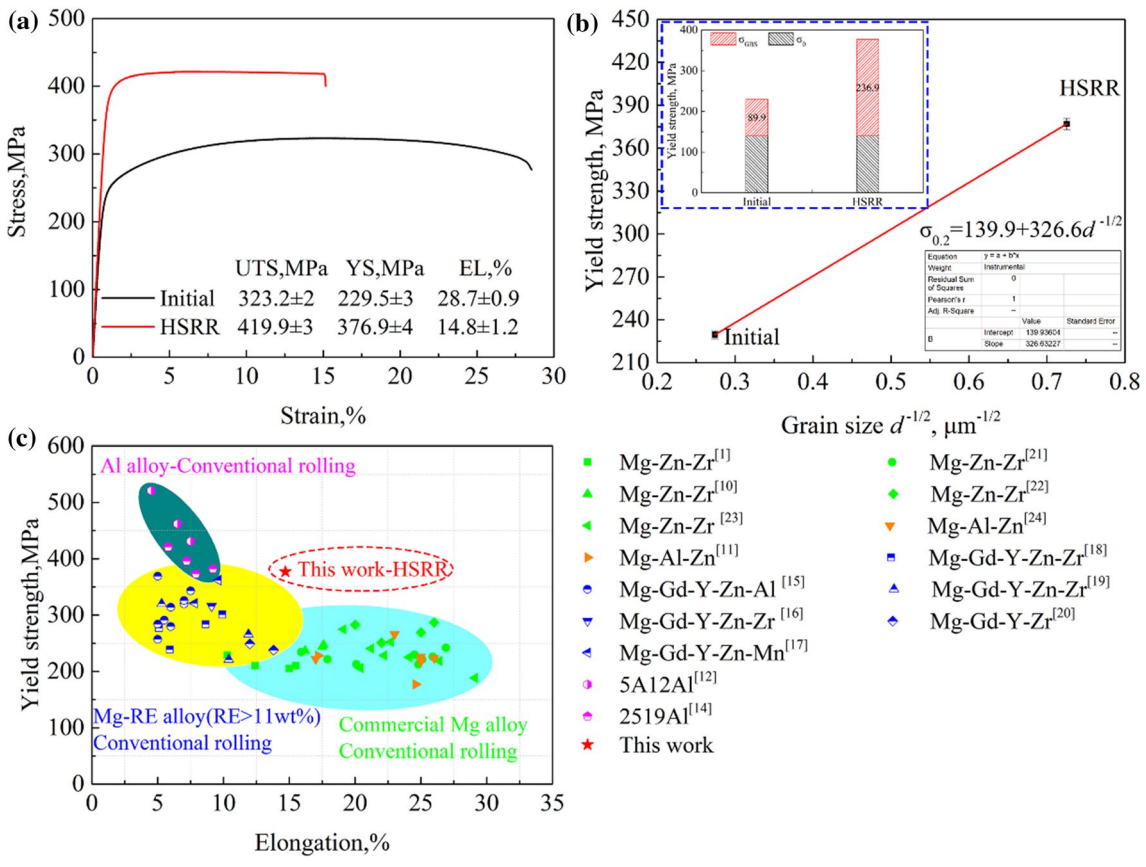

Fig. 1 **a** Stress–strain curves of the ZK60 alloy sheets, **b** Hall–petch relationship and **c** comparison of yield strength and elongation among Al, RE-Mg and commercial Mg alloys

(including texture state, dislocation density and precipitation). The relationship between yield strength and grain size ($d^{-1/2}$) of the alloy in the initial and HSRRed sheets were fitted, as shown in Fig. 1b. The parameters σ_0 was 139.9 MPa, and slope k was 326.6 MPa·μm $^{1/2}$, which was basically consistent with the research results (σ_0: 10 ~ 131 MPa, k: 160 ~ 348 MPa·μm $^{1/2}$) of Yuan et al. [13]. Specifically, the yield strength could be written as: $\sigma_{0.2} \approx 139.9\ \text{MPa} + 326.6\ \text{MPa}\cdot\mu\text{m}^{1/2} d^{-1/2}$. Grain refinement contributes about 89.5 MPa and 236.9 MPa to yield strength of initial and HSRRed sheets, respectively (The blue rectangle was shown by the dotted line in Fig. 1b). Figure 1c summarizes the YS and EL of conventional rolling Al [12, 14], Mg-RE [15–20] and commercial Mg alloy [1, 10, 11, 21–24]. Compared with the conventional rolled (CR) 5A12 and 2519Al, the strength (373 MPa ~) of the HSRRed sheet was slightly lower, but the plasticity was significantly higher than that of the Al alloy (~ 9.2%). CRed commercial Mg alloys have low strength(~ 250 MPa) but good ductility (~ 25%). However, the strength and ductility of the HSRRed sheet were higher than those of CRed the Mg-RE alloy sheets. As discussed above, the HRSSed ZK60 alloy sheet exhibited excellent mechanical properties at room temperature and had an extensive application prospect.

Figure 2 depicts the microstructure characteristics of the ZK60 alloy. In this work, Grain orientation spread (GOS) values less than 2 (blue and green) were considered as dynamic recrystallized (DRXed) grains, and GOS values greater than 2 (brown and yellow) were considered as deformed (unDRXed) grains [25]. Clearly, the initial sheet exhibited the duplex structure characteristics of large unDRXed grains and small DRXed grains (red arrow in Fig. 2a) with an average grain size of 13.3 μm. The results showed an insufficient DRX process during extrusion (DRX ratio was 55.1%) [1]. However, after HSRRed, the coarse grains have been significantly refined with a grain size of 1.9 μm, and the grain size distribution was well fitted the Gaussian distribution function, indicating that HSRR could not only effectively refine the microstructure, but also improve the microstructure uniformity of the rolled sheets. These results showed that DRX occurred almost completely during HSRR (DRX reaches 96.5%). According to Zener-Hollomon parameters, the lower the deformation temperature, the higher the Z value and the smaller the DRXed size [1]. In fact, low-temperature rolling not only increased DRX nucleation sites by introducing more energy storage but also inhibited the rapid migration of high-angle grain boundaries. Additionally, the misorientation angle distribution in Fig. 2c and f presents a high peak at 30°. As reported, about the high

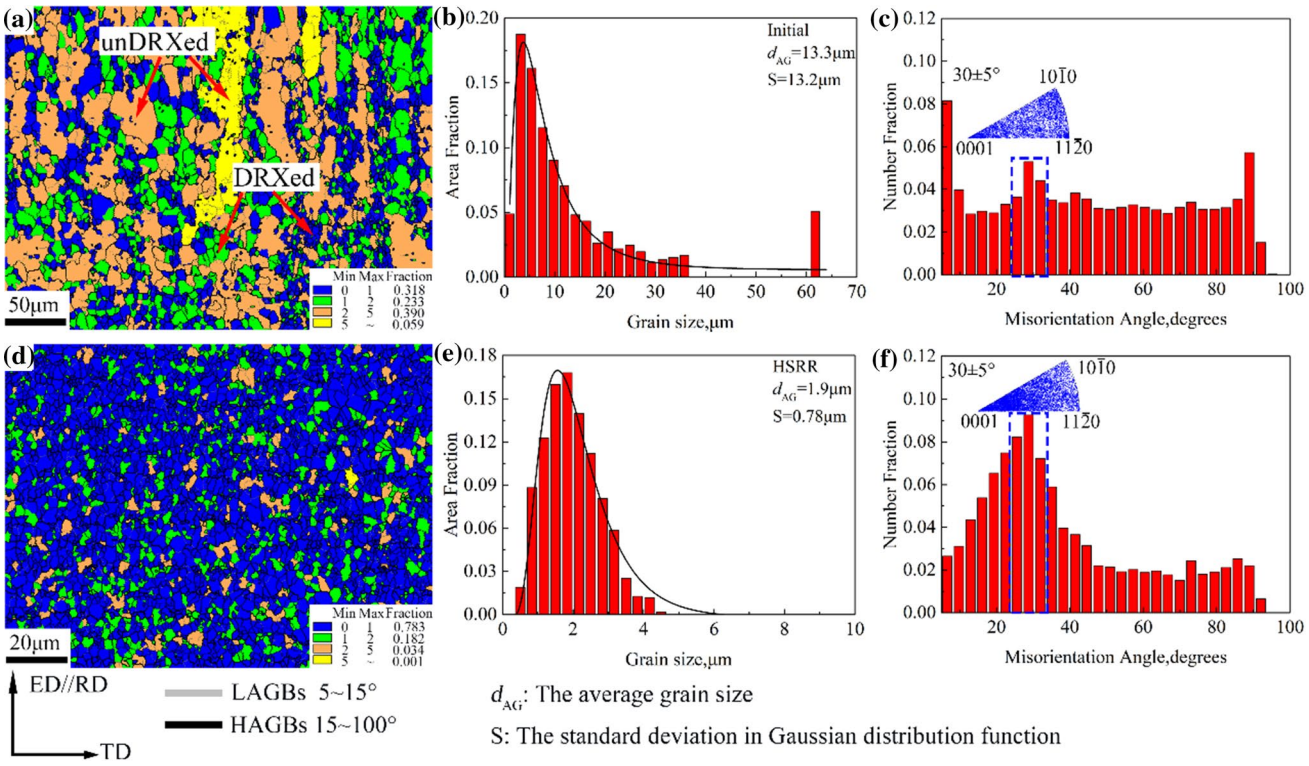

Fig. 2 Microstructure characteristics of the ZK60 alloy sheets, **a–c** Initial, **d–f** HSRR; **a**, **d** GOS, **b**, **e** Grain size distribution, **c**, **f** Misorientation angle. *ED* extrusion direction, *RD* rolling direction, *TD* transverse direction

peak at 30°, Imandoust et al. [26] attributed to the rotation of crystal lattice around < 0001 > produced by prismatic slip during DRX. Prismatic slips were activated and rotated crystal orientation around < 0001 > about 30° during the DRX process as reported in the extruded Mg alloys [27].

Figure 3 presents the Kernel Average Misorientation (KAM) map of the ZK60 alloy. KAM represented the geometrically necessary dislocations density (ρ_{GNDS}) distribution and orientation gradient in the grains. The ρ_{GNDS} could be expressed as [25, 27]:$\rho_{GNDs} = 2\Theta/ub$, where Θ was the average misorientation, b was the Burgers vector (0.32 nm) and u was the unite length of the point, which was equal to scan step size (0.3 μm). Θ was evaluated from the local misorientation profile in the KAM map (Fig. 3c, d). According to the Θ values (0.765448° (Initial), and 0.593083° (HSRR)), the ρ_{GNDS} densities of Initial, and HSRR were about 2.783 $\times 10^{15} m^2$ and 2.156 $\times 10^{15} m^2$, respectively. In Fig. 3, the distribution of local orientation deviation was not uniform, and the orientation deviation at the grain boundary was generally higher than that inside grain [27]. These results indicated that the dislocation accumulation at the grain boundary was severe and the deformation storage was large, which provided the energy for the nucleation of DRX. After HSRRed, the local misorientation deviation and ρ_{GNDs} decreased. The reduction of local misorientation deviation and ρ_{GNDs} was attributed to the cross slipping and dislocation climbing [25, 27].

Figure 4 reveals the pole figures and basal pole density of the ZK60 alloy sheets. In Fig. 4a, the (0002) basal plane of the initial sheet was almost parallel to the ED-normal direction (ND) plane. The maximum pole density of the initial sheet was 13.7 in the angle range of 78.8–90° along the RD and obviously strengthened to 36.1 in the angle range of 0–39.4° along the TD. The (10–10) and (11–20) crystal planes were symmetric about TD, which was typical (11–20) < 10–10 > texture [1]. After HSRRed, the texture of the sheet still showed a strong basal texture that the maximum texture density increased from 10.2 to 14.0, but the texture state was different from that of the initial sheet. Specifically, the c-axis was deflected from parallel to the ND of the rolled sheet, and in the angle range of 70.1–90° along the RD, which was similar to the initial sheet but more diffuse. However, the orientation distribution in the TD was obviously different from that of the initial sheet,

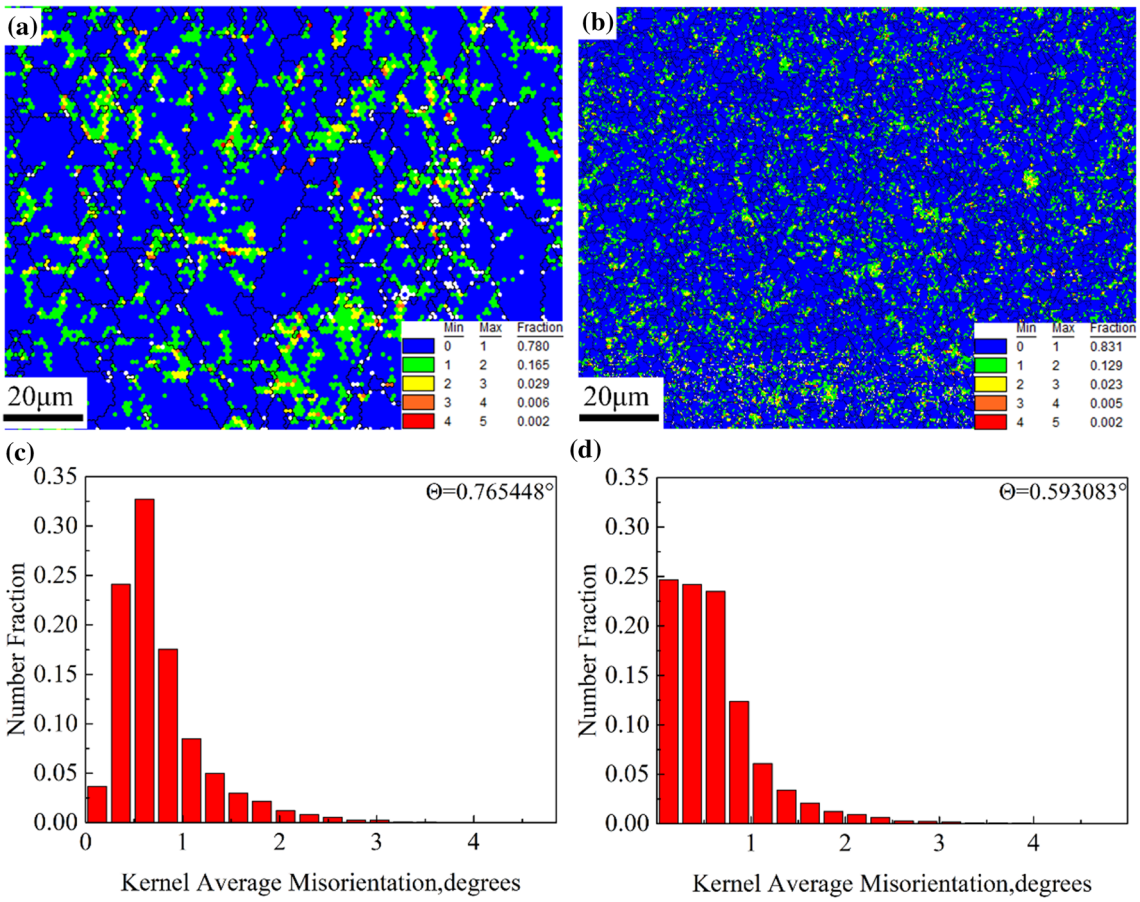

Fig. 3 Kernel Average Misorientation maps of the ZK60 alloys, **a**, **c** Initial **b**, **d** HSRR

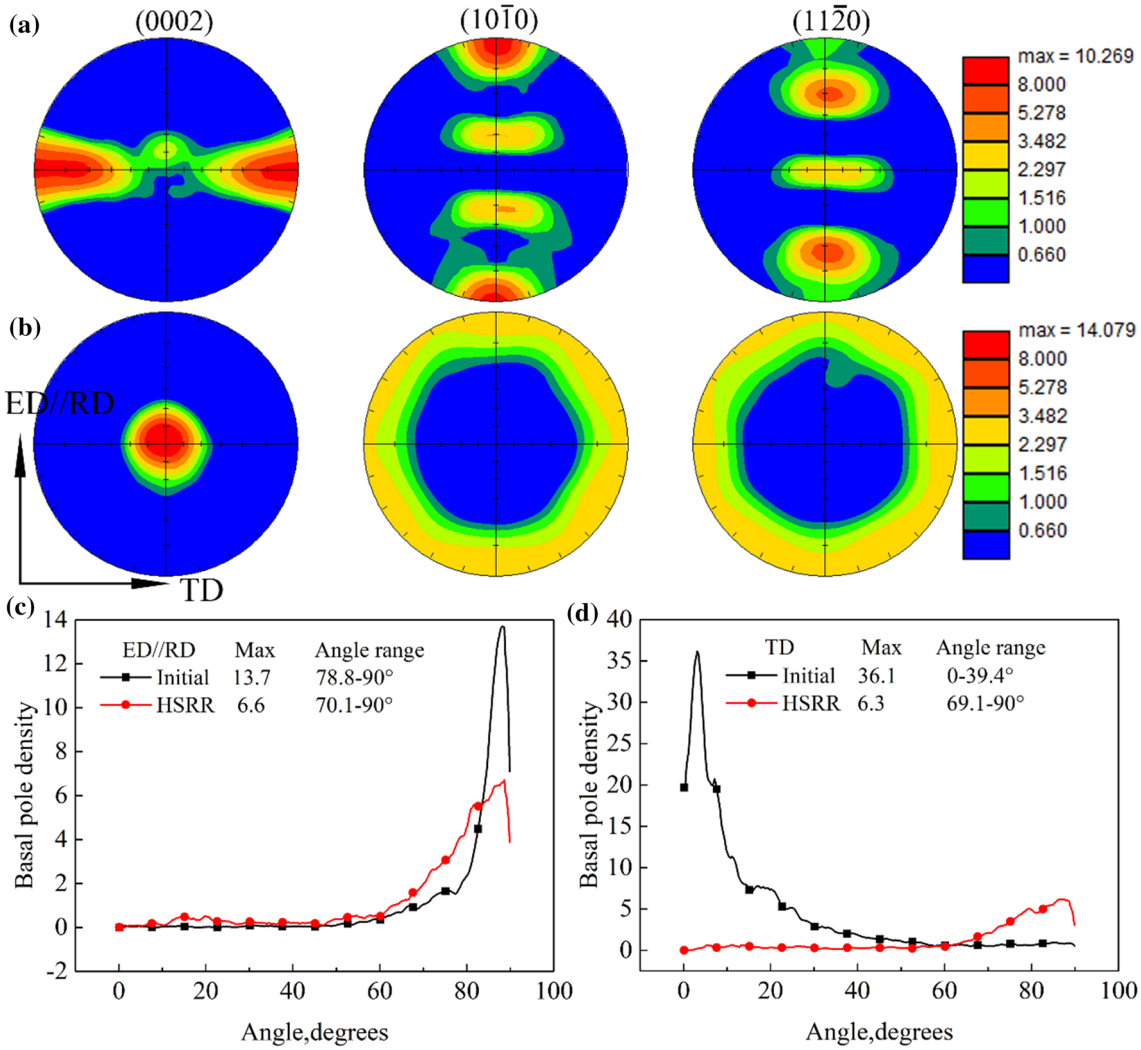

Fig. 4 Pole figures and basal pole density of the ZK60 alloy sheets, **a** Initial **b** HSRR, **c** ED//RD, **d** TD

and in the angle range of 69.1–90° along the TD. In general, after HSRRed, the grain orientation distribution in the RD becomes more diffuse, while changes in the TD and the distribution were more concentrated.

Figure 5 illustrates the Schmid factors (SF) of the ZK60 alloy sheets. As known, Mg alloys were mainly basal slip at room temperature [7]. In addition, grain refinement was favorable to the activation of prismatic slip and pyramidal slip during deformation [10]. Obviously, basal < a > slip (0.172), prismatic < a > (0.449), and pyramidal < c + a > slips (0.429) of the HSRRed sheet were much higher than those of the initial sheet. Compared with the initial sheet texture, the basal texture of the HSRR sheet was weakened in RD due to the DRX. In other words, the c-axis direction of the grain deviates from the ND. And the SF of the basal slip system in the grain increased and the basal slip was easier to activate when the tensile was carried out along the RD of the HSRR sheet. Therefore, the HSRRed sheet exhibited good plasticity.

There were two effects of grain refinement on sheet metal formability: First, grain refinement could increase the coordinated deformation ability of grains, reduce the stress concentration at grain boundaries, and delay the initiation and propagation of cracks along grain boundaries. Second, grain refinement was also beneficial to the activation of multi-slip systems. Although the basal slip was the most important slip system of Mg alloys at room temperature, when the grains of AZ31 alloy were refined to 6 μm, the amorphous slip and the cross slip from the basal slip to the non-basal slip occurred [28]. At this time, the prismatic-slip CRSS/basal-slip CRSS was only 1.1, which was much lower than that of single-crystal Mg alloy (~ 100). In other words, grain refinement was beneficial to the activation of multiple slip systems during Mg alloy deformation

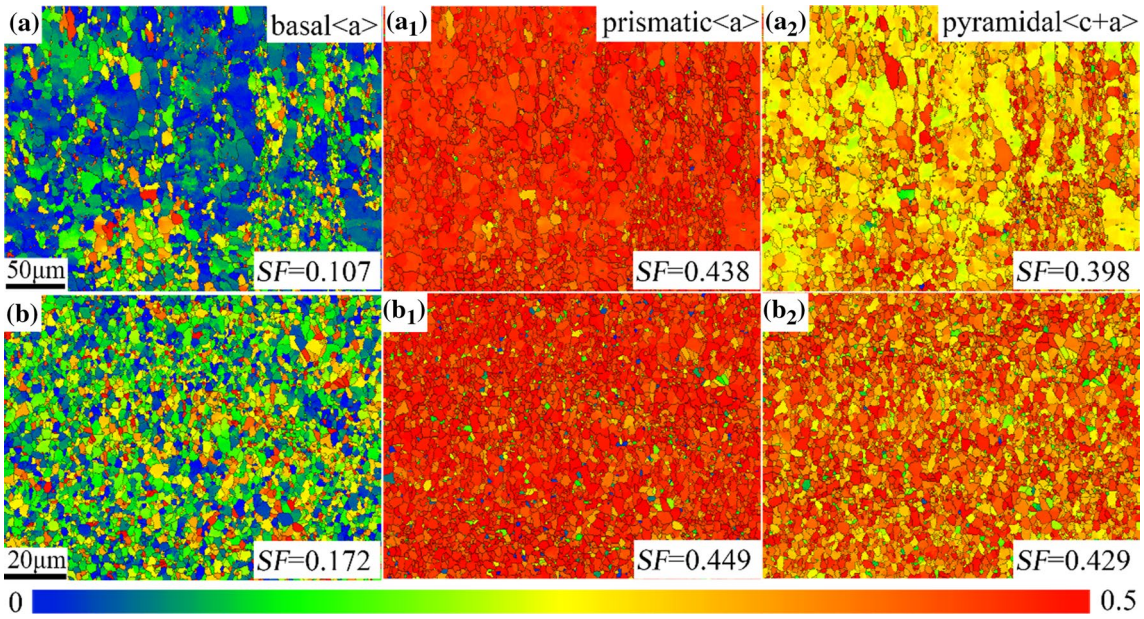

Fig. 5 Schmid factors of the ZK60 alloy sheets: **a**, $\mathbf{a}_1$, $\mathbf{a}_2$ Initial, **b**, $\mathbf{b}_1$, $\mathbf{b}_2$ HSRR

by coordinating the plastic deformation, thus improving the plastic deformation capacity of the Mg alloy. In addition, the reduction of dislocation density caused by DRXed was also conducive to the progress of dislocation slip in the subsequent deformation process, reducing the dislocation plug degree. Therefore, grain refinement and defect density reduction caused by large-scale DRX in the HSRRed process were beneficial to improve the plasticity and make the sheet has high elongation.

In traditional plastic processing, because DRX was a softening process, the dislocation density in recrystallized grain was very low, and the strain hardening effect in the process will be weakened [10]. When the DRX degree was very high, most of the strain hardening region would be replaced by the recrystallization region, and the strength of the material would decrease. In fact, the strength of the HSRRed sheet was still higher than that of the initial sheet. Obviously, there were other strengthening factors in the HSRRed sheet. For instance, fine-grain strengthening was an important strengthening mechanism because the DRXed grains in the HSRRed sheet were very uniform and fine. In conclusion, large area DRX has two effects on the strength of the HSRRed sheet. (1) the weakening of the strain-hardening was caused by the reduction of dislocation density; (2) the fine uniform recrystallized grains led to the fine-grain strengthening effect. Since the Hall–Petch slope (k) of the HCP crystals was larger than that of the FCC and BCC metals, grain refinement has a greater effect on the strength of the Mg alloys [13, 29]. When the grain was refined to a certain extent, the strengthening effect of fine grain exceeded the weakened effect caused by dislocation reduction, and the material could obtain high strength.

The HSRRed sheet has good comprehensive mechanical properties, which were mainly affected by grain size, dislocation density and texture. More specific: (1) Relatively uniform fine grains could be obtained by HSRRed in sheet, and fine grains could obtain high strength and high plasticity simultaneously in the sheet. (2) The smaller the grain size, the more the number of grains per unit volume, so that the deformation could be dispersed in more grains, and the coordinated deformation ability of grains was enhanced. Grain refinement could also shortened the length of dislocation slip path and dislocation plug group, reduced stress concentration near grain boundaries, and improved plasticity. (3) The texture of {0002} basal still existed in the HSRRed sheet, but the texture composition did not change fundamentally. However, due to the DRX, the basal texture of the HSRR sheet was weakened in RD compared with the initial sheet texture. However, when the texture of the basal in RD was weakened, the c-axis direction of the grain deviated from the ND of the sheet, the SF of the basal slip system in the grain increased and the basal slip was easier to start, which improves the plasticity of the material. In conclusion, grain refinement could improve the strength of the sheet, and dislocation density reduction and RD texture weakening could improve the plasticity of the sheet, so the HSRRed sheet showed ultra-high-strength and good ductility.

4 Conclusions

In this work, the effects on the microstructure evolution, texture and mechanical properties of the ZK60 sheet by the high strain rate rolling were investigated, the main conclusions were as follows:

HSRRed sheet has good comprehensive mechanical properties (the ultimate tensile strength of 419.9 ± 3 MPa, the yield strength of 376.9 ± 4 MPa and the elongation of $14.8 \pm 1.2\%$), which were mainly affected by grain size, dislocation density and texture. Relatively uniform fine grains (~ 1.9 μm) could be obtained by HSRR, and fine grain strengthening plays a leading role. The smaller the grain size, the more grains per unit volume, so that the deformation could be dispersed in more grains, and the coordinated deformation ability of grains was enhanced. Grain refinement can also shorten the length of dislocation slip path and dislocation plug group, and reduce stress concentration near grain boundaries, thereby improved plasticity. The HSRRed sheet has completely dynamic recrystallization (96.5%), the basal texture in the RD has been weakened to a certain extent, and the c-axis direction of the grain deviated from the normal direction of the plate. During the subsequent tensile along the RD, the Schmid factor of the basal slip system in the grain increased, the basal slip was easier to activate, and the plasticity of the material was improved.

Acknowledgements This work was supported by Key Research and Development Plan in Shandong Province (2019JZZY010364 and 2020CXGC010303), Initial Scientific Research Fund of Shandong Jiaotong University (Grant No. BS201902056), the State Key Program of National Natural Science Foundation of China (Grant No. U1937205), the National Natural Science Foundation of China (Grant No. 51775134).

Author's contribution SW: Conceptualization, writing-original draft, formal analysis, carried out the experiment, planned the experiments. JY, XD: conceptualization, writing-original draft, formal analysis, planned the experiments. JP, XJ: carried out the experiment. WZ: supervision, planned the experiments.

Declarations

Conflict of interest The authors declare that they have no known competing financial interests or personal relationships that could have appeared to influence the work reported in this paper.

References

1. W.K. Wang, W.Z. Chen, W.C. Zhang, G.R. Cui, E.D. Wang, Mater. Sci. Eng. A **712**, 608–615 (2018)
2. R.X. Zheng, J.P. Du, S. Gao, H. Somekawa, S. Ogata, N. Tsuji, Acta Mater. **198**, 35–46 (2020)
3. M. Markushev, D. Nugmanov, O. Sitdikov, A. Vinogradov, Mater. Sci. Eng. A **709**, 330–338 (2018)
4. X. Liu, H. Yang, B.W. Zhu, Y.Z. Wu, W.H. Liu, C.P. Tang, J. Magnes. Alloy. **10**, 1096–1108 (2022)
5. D. Orlov, G. Raab, T.T. Lamark, M. Popov, Y. Estrin, Acta Mater. **59**, 375–385 (2011)
6. W.T. Sun, X.G. Qiao, M.Y. Zheng, C. Xu, S. Kamado, X.J. Zhao, H.W. Chen, N. Gao, M.J. Starink, Acta Mater. **151**, 260–270 (2018)
7. S.Q. Zhu, H.G. Yan, J.H. Chen, Y.Z. Wu, J.Z. Liu, J. Tian, Scripta Mater. **63**, 985–988 (2010)
8. Y. Xu, X.X. Zhang, W. Li, P.H. Hu, J.B. Jia, J.T. Luo, Mater. Sci. Eng. A **781**, 139221 (2020)
9. J.M. Jiang, J. Wu, S. Ni, H.G. Yan, M. Song, Mater. Sci. Eng. A **712**, 478–484 (2018)
10. S.Q. Zhu, H.G. Yan, J.H. Chen, Y.Z. Wu, B. Su, Y.G. Du, X.Z. Liao, Scripta Mater. **67**, 404–407 (2012)
11. S.Q. Zhu, H.G. Yan, J.H. Chen, Y.Z. Wu, Y.G. Du, X.Z. Liao, Mater. Sci. Eng. A **559**, 765–772 (2013)
12. X.Y. Li, W.J. Xia, H.G. Yan, J.H. Chen, B. Su, M. Song, Z.Z. Li, Y. Lu, Mater. Sci. Eng. A **787**, 139481 (2020)
13. W. Yuan, S.K. Panigrahi, J.Q. Su, R.S. Mishra, Scripta Mater. **65**, 994–997 (2011)
14. I.S. Zuiko, S. Mironov, R. Kaibyshev, Mater. Sci. Eng. A **745**, 82–89 (2019)
15. C. Xu, M.Y. Zheng, K. Wu, E.D. Wang, G.H. Fan, S.W. Xu, S. Kamado, X.D. Liu, G.J. Wang, X.Y. Lv, Mater. Sci. Eng. A **559**, 615–622 (2013)
16. Z.B. Chen, C.M. Liu, H.C. Xiao, J.K. Wang, Z.Y. Chen, S.N. Jiang, Z.J. Su, Mater. Sci. Eng. A **618**, 232–237 (2014)
17. C. Xu, M.Y. Zheng, S.W. Xu, K. Wu, E.D. Wang, G.H. Fan, S. Kamado, Mater. Sci. Eng. A **643**, 137–141 (2015)
18. B. Li, B.G. Teng, E.D. Wang, Mater. Sci. Eng. A **765**, 138317 (2019)
19. K. Wang, J.F. Wang, X. Peng, S.Q. Gao, H. Hu, L.J. Zeng, F.S. Pan, Mater. Sci. Eng. A **748**, 100–107 (2019)
20. S.Q. Liu, M. Han, Z.H. Huang, Z.M. Zhang, C.J. Xu, X. Li, F. Chen, Z.Q. Yan, F.Y. Kong, A.D. Wang, Z.X. Liu, J. Alloy. Compd. **901**, 163667 (2022)
21. L.X. Zhang, W.Z. Chen, W.C. Zhang, W.K. Wang, E.D. Wang, J. Mater. Process. Tech. **237**, 65–74 (2016)
22. W.Z. Chen, L.M. Ma, X.M. Chen, G.R. Cui, W.C. Zhang, E.D. Wang, Mater. Sci. Eng. A **733**, 350–360 (2018)
23. W.Z. Chen, Y. Yu, X. Wang, E.D. Wang, Z.Y. Liu, Mater. Sci. Eng. A **575**, 136–143 (2013)
24. J.R. Li, D.S. Xie, H.S. Yu, R.L. Liu, Y.Z. Shen, X.S. Zhang, C.G. Yang, L.F. Ma, H.C. Pan, G.W. Qin, J. Alloy. Compd. **835**, 155228 (2020)
25. S.H. Wang, W.C. Zhang, H.X. Wang, J.L. Yang, W.Z. Chen, G.R. Cui, G.F. Wang, Mater. Sci. Eng. A **803**, 140488 (2021)
26. A. Imandoust, C. Barrett, A. Oppedal, W. Whittington, Y. Paudel, H. Kadiri, Acta Mater. **138**, 27–41 (2017)
27. H.C. Pan, R. Kang, J.R. Li, H.B. Xie, Z.R. Zeng, Q.Y. Huang, C.L. Yang, Y.P. Ren, G.W. Qin, Acta Mater. **186**, 278–290 (2020)
28. J. Koike, T. Kobayashi, T. Mukai, H. Watanabe, M. Suzuki, K. Maruyama, K. Higashi, Acta Mater. **51**, 2055–2065 (2003)
29. H.H. Yu, C.Z. Li, Y.C. Xin, A. Chapuis, X.X. Huang, Q. Liu, Acta Mater. **128**, 313–326 (2017)